Available online at www.sciencedirect.com
ScienceDirect
Trans. Nonferrous Met. Soc. China 32(2022) 1677−1690
Transactions of Nonferrous Metals Society of China
www.tnmsc.cn

Priority recovery of lithium and effective leaching of nickel and cobalt from spent lithium-ion battery

Ning CAO, Ya-li ZHANG, Lin-lin CHEN, Yun JIA, Yao-guo HUANG

School of Chemistry and Chemical Engineering, Shandong University of Technology, Zibo 255049, China

Received 23 March 2021; accepted 8 October 2021

Abstract: The cathode materials of spent lithium-ion batteries (LIBs) were recovered via reductive roasting, Na_2CO_3 leaching, and ammonia leaching. The effects of roasting parameters, Na_2CO_3 leaching parameters, and ammonia leaching parameters on the leaching efficiencies of metals were explored. The results show that the mineral phase of spent LIBs is reconstructed during reductive roasting, and more than 99% of Li can be preferentially leached via Na_2CO_3 leaching. Ni (99.7%) and Co (99.9%) can be leached via one-step ammonia leaching, and Mn cannot be leached. Thus, good leaching selectivity is achieved. The kinetic study shows that the leaching of Ni and Co conforms to chemical reaction control.

Key words: lithium; priority recovery; reductive roasting; ammonia leaching; spent lithium-ion battery

1 Introduction

The lithium-ion battery (LIB) industry has developed rapidly with the support of the new alternative energy automobile industry. Lithium-ion battery production reached 3.74 million tons in 2016, according to relevant reports [1]. The rapid development of LIBs has led to the emergence of a larger number of spent LIBs. It has been estimated that the end-of-life LIBs will reach approximately 11 million tons by 2030 [2]. End-of-life LIBs contain heavy metals (Ni, Co, Mn, Li, Al, etc.) and electrolytes, which are all harmful substances. If the batteries were discarded directly without treatment, the environment would become severely polluted, and human survival would also be threatened [3]. At the same time, with the widespread use of LIBs, the demand for the raw materials obtained from them, including valuable metals, has also increased sharply. Valuable metals in spent LIBs provide important raw materials to be reused. If an effective method is developed to retrieve valuable metals from spent LIBs, it would provide an important benefit for environmental protection and the possibility to reuse valuable resources.

The recovery and treatment of spent LIBs has already been studied extensively [4,5]. The hydrometallurgical recovery of cathode materials has aroused widespread attention [6,7] because of its low energy consumption and benefit to the environment. Valuable metals such as Ni, Co, Mn, Li, Cu, and Al are leached by acid [8]. H_2SO_4 [9] and citric acid [10] are generally used to leach valuable metals, with high leaching efficiency. However, acid leaching is applied to leaching most metals with poor selectivity, which increases the costs of subsequent separation and purification, and strong acids cause corrosion of the equipment. The ammonia leaching method has aroused considerable concern due to its high selectivity [11]. Metals such as Ni, Co, Li, and Cu, which can be complexed with ammonia, are leached, while other metals such as Mn and Al are not leached. WANG et al [8]

Corresponding author: Ya-li ZHANG, E-mail: zhangyali@sdut.edu.cn
DOI: 10.1016/S1003-6326(22)65902-8

developed a reduction-ammoniacal method and used ammonia, ammonium salts, and reduction agents to leach metals. In total, 100% Co, 98.3% Ni, and 90.3% Li were dissolved within the solutions. QI et al [12] proposed an ammonia leaching method and used an $NH_3·H_2O$−NH_4HCO_3−Na_2SO_3 solution to leach Co and Li, with leaching efficiencies of 91.16% and 97.57%, respectively. WU et al [13] used a ternary leaching system (NH_3−$(NH_4)_2SO_3$−NH_4HCO_3) to leach Li, Ni, Co, Cu, and Al. In their study, Li, Co, Ni, and Cu achieved high leaching efficiencies, whereas Al was barely leached. WANG et al [14] proposed an NH_3−$(NH_4)_2CO_3$−Na_2SO_3 leaching system, and 79.1% of Li, 86.4% of Co, and 85.3% of Ni were selectively leached.

The above study indicated that Ni, Co, Li, and Cu could be selectively leached by a system of ammonia, ammonium salts, and reducing agents. However, similar to acid leaching, Li is leached together with Ni and Co, and the separation of Li from nickel−cobalt is expected to cause a loss of Li. The prioritized recovery of Li causes a technical bottleneck for the efficient recovery of Li; meanwhile, the leaching efficiencies of metals are not high. MA et al [15] preferentially leached Li through carbothermic reduction−water immersion, and then Ni and Co were leached using the ammonia leaching method. However, the leaching efficiency of Li was only 82.2%, and 97.7% Ni and 99.1% Co could be selectively leached by $NH_3·H_2O$ and $(NH_4)_2SO_3$. Therefore, the leaching efficiencies of Li and Ni need to be improved.

In this study, $(NH_4)_2SO_3$ was used as the reducing agent to reconstruct the mineral phase through reductive roasting. Li was preferentially recovered by Na_2CO_3 leaching, which prevented the loss of Li^+ during the subsequent separation process. The mechanism of phase transformation was analyzed and discussed based on the morphology and valence state of the pre-roasted and post-roasted cathode materials. Ni and Co were selectively leached by ammonia leaching, and Mn was recovered as $MnCO_3$. The kinetics of Ni and Co during ammonia leaching were studied. In addition, the effects of different reductive roasting conditions and leaching conditions on Li, Ni, and Co were also investigated, and the recovered Li_2CO_3 and $MnCO_3$ were characterized and analyzed.

2 Experimental

2.1 Materials and analysis

The cathode material used in this study was $Li(Ni_xCo_yMn_z)O_2$, which was provided by an LIB recovery company in Guangzhou, China. After crushing, the spent cathode material was first roasted in a muffle furnace at 550 °C for 1 h to separate the active material from the Al foil and remove the binder and conductive agent [16]. Then, the active material was passed through a 325-mesh sieve, and the metal content was measured by atomic absorption spectroscopy (AAS, TAS−990F). The results are presented in Table 1. All reagents used in this study were of analytical grade, and the solutions were diluted with deionized water.

Table 1 Contents of metals in spent cathode material (wt.%)

Ni	Co	Mn	Li	Al	Cu*
17.2	6.2	35.2	6.3	0.72	0.08

*−mg/g

2.2 Mineral phase reconstruction by roasting

Mineral phase reconstruction of the cathode materials was carried out by roasting, and Li was preferentially leached in a sodium carbonate solution, with priority recovery of Li achieved. The cathode materials and $(NH_4)_2SO_3$ were uniformly mixed and roasted in a tube furnace in a N_2 atmosphere at 550 °C for 150 min. To study the effect of the roasting process on the mineral phase reconstruction, the pre-roasted and post-roasted cathode materials were characterized and analyzed using a scanning electron microscopy (SEM, Quanta 250) with energy-dispersive X-ray spectroscopy (EDS), X-ray diffraction (XRD, Bruker AXS D8 Advance), and X-ray photoelectron spectroscopy (XPS, Thermo ESCALAB 250XI). The effect of the additive ($(NH_4)_2SO_3$) on the leaching efficiency of Li was investigated under the same Na_2CO_3 leaching conditions: a liquid-to-solid ratio of 50:1, a leaching temperature of 0 °C, a molar ratio of 1:1.3 for the cathode materials and Na_2CO_3, and a treatment period of 3 h.

2.3 Recovery of lithium

The post-roasted cathode materials and Na_2CO_3 were first added into a round bottom flask at specific molar ratios (1:0, 1:1, 1:1.3, and 1:1.5) and then leached for set time periods (2, 2.5, 3, and 3.5 h) for different liquid-to-solid ratios (20:1, 40:1, 50:1, 60:1, and 80:1) at 0 °C. The mixture was filtered immediately after reaching the reaction time, and the filter cake was washed three times with deionized water at 0 °C. The metal content in the leachate was measured by AAS, and the leaching efficiencies (%) of metal ions were calculated using Eq. (1):

$$x=\frac{cV}{m_0 w_0}\times 100\% \quad (1)$$

where m_0 (g) is the mass of the cathode materials used in this experiment, w_0 (%) is the metal ion content in the cathode material, c (g/L) is the concentration of metal ions in the leachate, and V (L) is the volume of leachate. The filter cake was first dried in a drying oven and then used in subsequent ammonia leaching experiments. Li_2CO_3 in the leachate was recovered by evaporation and concentration, and the recovered Li_2CO_3 was characterized by XRD. The leaching residue was characterized using XRD and SEM.

2.4 Recovery of Ni and Co

Ammonia leaching experiments were carried out in a three-necked flask equipped with a reflux device. The dried Na_2CO_3 leaching residue was added to the ammonia leaching solution according to a liquid-to-solid ratio (20:1, 30:1, 40:1, 50:1, 60:1, 80:1, and 100:1). The ammonia leaching solution was composed of $NH_3{\cdot}H_2O$ (2, 3, 4, and 5 mol/L), $(NH_4)_2CO_3$ (1, 2, 2.5, 3, and 4 mol/L), Na_2SO_3 (0.1, 0.2, 0.3, 0.4, and 0.5 mol/L) and deionized water. Ammonia leaching experiments were carried out at specific temperatures (20, 40, 60, and 80 °C) as well as for a prescribed time (1, 2, 3, 4, 5, and 6 h). The ammonia leachate was filtered immediately after reaching the reaction time, and the filter cake was washed three times. The metal ion content in the ammonia leaching solution was measured by AAS, and the leaching efficiency of metals was calculated using Eq. (1). The ammonia leaching residue was dried in a drying oven and analyzed by XRD.

3 Results and discussion

3.1 Priority recovery of lithium

3.1.1 Characterization and analysis of pre-roasted and post-roasted cathode materials

The pre-roasted and post-roasted cathode materials were characterized by XRD, SEM, EDS and XPS. The XRD patterns of the pre-roasted and post-roasted cathode materials are shown in Figs. 1(a, b), respectively. The crystal plane diffraction peaks of the pre-roasted cathode materials were consistent with those of standard $Li(Ni_xCo_yMn_z)O_2$. However, these diffraction peaks were not observed in the post-roasted cathode materials; obvious diffraction peaks of Li_2SO_4, $CoSO_4$, $NiSO_4$, Co_3O_4, MnO_2, and $(NiO)_m{\cdot}(MnO)_n$ are shown in Fig. 1(b).

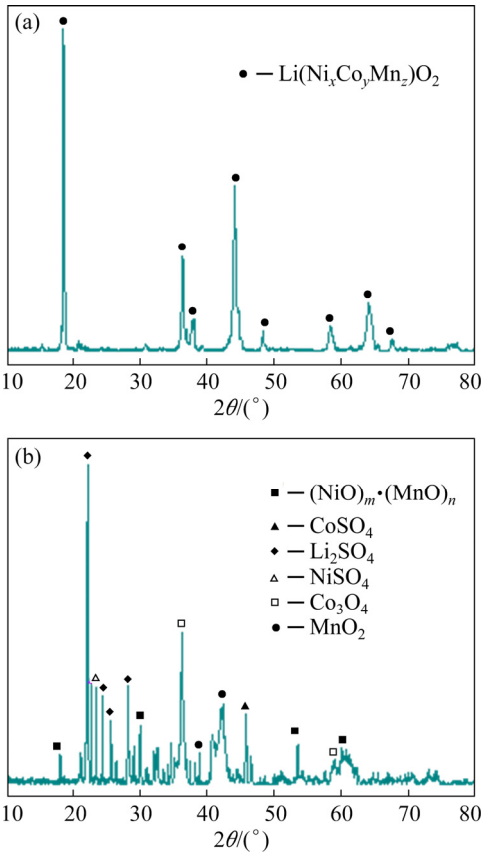

Fig. 1 XRD patterns of pre-roasted (a) and post-roasted (b) cathode materials

The morphologies of the pre-roasted and post-roasted cathode materials were characterized by SEM, as shown in Figs. 2(a, c), respectively. The EDS results are shown in Figs. 2(b, d), respectively. From Figs. 2(a, c), it can be seen that the

morphology of the pre-roasted cathode materials was spherical and the surface was relatively smooth. However, the spherical structure was destroyed after roasting, and the surface became rough. It can be observed from Figs. 2(b, d) that Ni, Co, and Mn were uniformly distributed on the surface of the cathode materials, while the distribution of Cu and Al was uneven and the amounts were small.

To further explore the change in the valence state of metals during reductive roasting, the pre-roasted and post-roasted cathode materials were analyzed by XPS. The Ni 2p spectra of the pre-roasted and post-roasted cathode materials are shown in Fig. 3(a). The binding energies of the main peaks for the pre-roasted cathode materials at Ni $2p_{3/2}$ and Ni $2p_{1/2}$ were 855.3 and 872.75 eV, respectively, and these peaks were attributed to Ni^{2+} [17]; The peaks at 861.86 and 879.88 eV corresponded to the satellite peaks of Ni $2p_{3/2}$ and Ni $2p_{1/2}$, respectively [18]. For the post-roasted cathode materials, the characteristic peaks at 855.3 and 873.69 eV corresponded to Ni^{2+} [19], revealing that the Ni element always existed in the divalent state, and had no change in valence state. The Co 2p spectra of the pre-roasted and post-roasted cathode materials are shown in Fig. 3(b). For the pre-roasted cathode materials, the major peaks of Co element with binding energies at 780.7 and 795.55 eV (Co $2p_{3/2}$ and Co $2p_{1/2}$) were assigned to Co^{3+} [20,21]. In the post-roasted cathode materials,

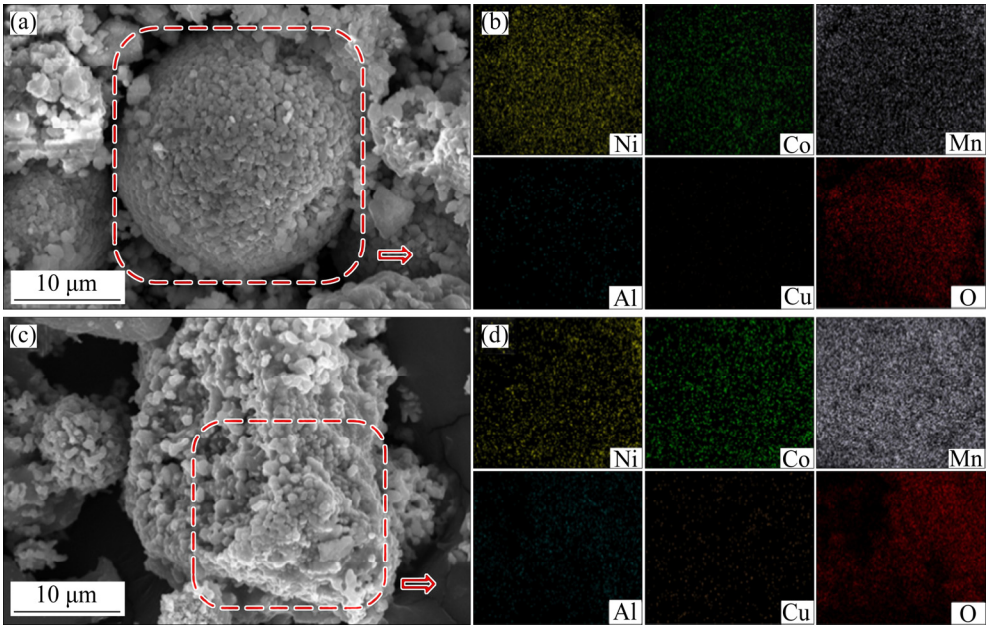

Fig. 2 SEM images (a, c) and EDS results (b, d) of pre-roasted (a, b) and post-roasted (c, d) cathode materials

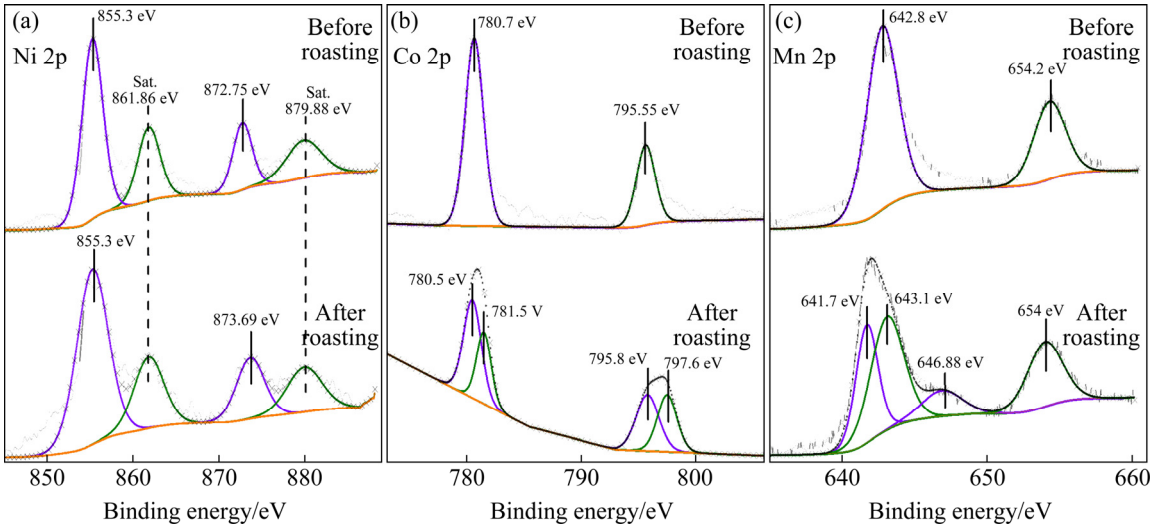

Fig. 3 XPS scans of Ni 2p (a), Co 2p (b), and Mn 2p (c) of pre-roasted and post-roasted cathode materials

the main peak of Co $2p_{3/2}$ was fitted by 780.5 and 781.5 eV, corresponding to Co^{3+} and Co^{2+} [22], respectively. This proved that part of the Co was reduced from trivalence to divalence after roasting. The Mn 2p spectra of the pre-roasted and post-roasted cathode materials are shown in Fig. 3(c). The peaks near 642.8 and 654.2 eV (Mn $2p_{3/2}$ and $2p_{1/2}$) in the pre-roasted cathode materials corresponded to Mn^{4+} [23,24]. The binding energies at Mn $2p_{3/2}$ of the post-roasted cathode materials were 641.7 and 643.1 eV, attributed to Mn^{2+} and Mn^{4+} [23,25], respectively; The binding energies at Mn $2p_{1/2}$ were 646.88 and 654 eV, and corresponded to Mn^{2+} and Mn^{4+} [24,26], respectively. Part of the Mn was reduced from tetravalence to divalence after roasting. The characterization results of XRD, SEM, and XPS proved that some metals were reduced by $(NH_4)_2SO_3$ during the roasting process, and the mineral phase structure of the cathode materials was reconstructed.

3.1.2 Mineral phase reconstruction of cathode materials during roasting process

The mineral phase reconstruction of the cathode materials during the roasting process is shown in Fig. 4. The uniformly mixed cathode materials and $(NH_4)_2SO_3$ were roasted in N_2 atmosphere. $(NH_4)_2SO_3$, which is easily decomposed by heat, produces SO_2. The trivalent Co and tetravalent Mn were reduced to a divalent state, and SO_2 was transformed into SO_4^{2-} when the cathode materials were in sufficient contact with SO_2. At the same time, as the frame structure of the cathode materials was destroyed, the stable chemical bond between the metals and oxygen atoms was also destroyed, and the Li escaped from the lattice. Ni^{2+}, Co^{2+}, and Mn^{2+} produced new substances with other elements, such as $CoSO_4$, $NiSO_4$, and $(NiO)_m{\cdot}(MnO)_n$. Co^{3+} and Mn^{4+} were not completely reduced owing to insufficient contact with SO_2 during roasting. The stable crystal structure was destroyed by the reduction reaction, and the unreduced metal ions combined with oxygen atoms to form Co_3O_4 and MnO_2.

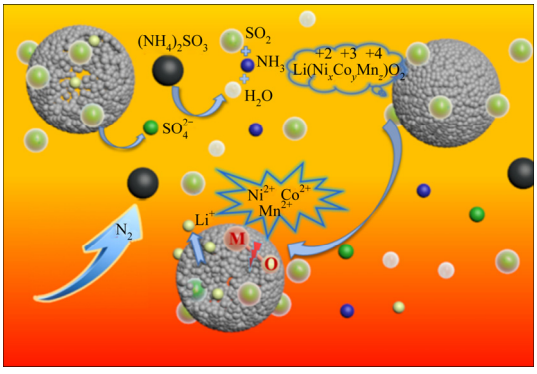

Fig. 4 Reductive roasting process

3.1.3 Effect of additive $(NH_4)_2SO_3$ dosage on leaching efficiency of Li during roasting

Lithium recovery was prioritized after roasting. To explore the effect of the reducing agent on the leaching efficiency of Li, the cathode materials were mixed with Na_2SO_3 and $(NH_4)_2SO_3$, respectively, at the same molar ratio (2:1) and then roasted in a tube furnace filled with N_2 at 550 °C for 150 min. After reductive roasting, the materials were leached under the same conditions (liquid-to-solid ratio of 30:1, leaching temperature of 0 °C, molar ratio of 1:1 for the cathode materials and Na_2CO_3, and leaching time of 2 h). The effects of different reducing agents on the leaching efficiency of Li are shown in Fig. 5(a). Compared with Na_2SO_3 (9%), the leaching efficiency of $(NH_4)_2SO_3$

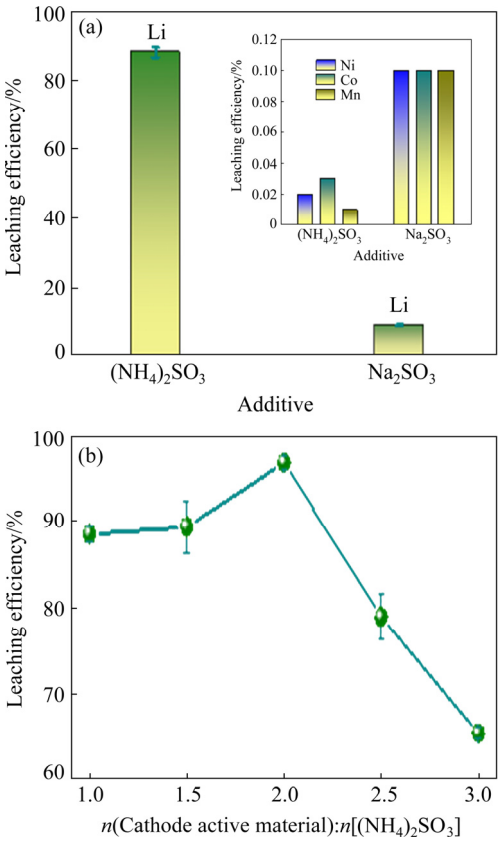

Fig. 5 Effects of $(NH_4)_2SO_3$ and Na_2SO_3 on leaching efficiencies of Ni, Co, Mn, and Li (molar ratio of cathode materials to additives of 2:1) (a) and effect of molar ratio of cathode materials to $(NH_4)_2SO_3$ on leaching efficiency of Li (b)

on Li was significantly higher, reaching 88%. The leaching efficiencies of Ni, Co, and Mn were all less than 0.03%. This was because $(NH_4)_2SO_3$ was thermally decomposed and produced a gas reduction during the roasting process, thereby increasing the reduction contact area with the cathode materials. The decomposition equation is shown in Reaction (2):

$$(NH_4)_2SO_3 \triangleq 2NH_3\uparrow + SO_2\uparrow + H_2O \quad (2)$$

Since Na_2SO_3 cannot be decomposed thermally, its ability to reduce cathode materials is poor. Therefore, $(NH_4)_2SO_3$ was selected as the reducing agent in subsequent experiments.

The effect of the $(NH_4)_2SO_3$ dosage on the leaching efficiency of Li is shown in Fig. 5(b). As the molar ratio of the cathode materials to $(NH_4)_2SO_3$ increased from 1:1 to 2:1, the leaching efficiency of Li also gradually increased. When the molar ratio was increased from 2:1 to 3:1, the leaching efficiency of Li decreased from 96.7% to 65.5%.

3.1.4 Effect of sodium carbonate leaching parameters on leaching efficiency of Li

Because the solubility of Li_2CO_3 decreased as the temperature increased [15], the optimal leaching temperature was selected as 0 °C. The effect of the leaching parameters on the Li leaching efficiency is shown in Fig. 6. As shown in Fig. 6(a), Li was recovered by water leaching (the molar ratio of cathode materials to Na_2CO_3 of 1:0) at liquid-to-solid ratio of 50:1, temperature of 0 °C, and leaching time of 3 h. In addition, 0.4% Ni, 0.86% Co, and 15.37% Mn were leached simultaneously. Ni^{2+}, Co^{2+}, and Mn^{2+} were converted to carbonate precipitates when Na_2CO_3 was added to the water leaching solution. Owing to the high solubility of Li_2CO_3 at 0 °C, it was found that Li could be preferentially recovered and separated from Ni, Co, and Mn. In addition, with the increase in Na_2CO_3 dosage, the leaching efficiency of Li progressively increased at first and then tended to level off. This was because more CO_3^{2-} promoted the precipitation of Ni^{2+}, Co^{2+}, and Mn^{2+}, and thereafter promoted the leaching of Li^+. When the molar ratio of cathode materials to Na_2CO_3 was 1:1.3, the leaching efficiency of Li^+ was high, reaching 98.1%.

The effect of the liquid-to-solid ratio on the leaching efficiency of Li was investigated. As shown in Fig. 6(b), the solution was not sufficient

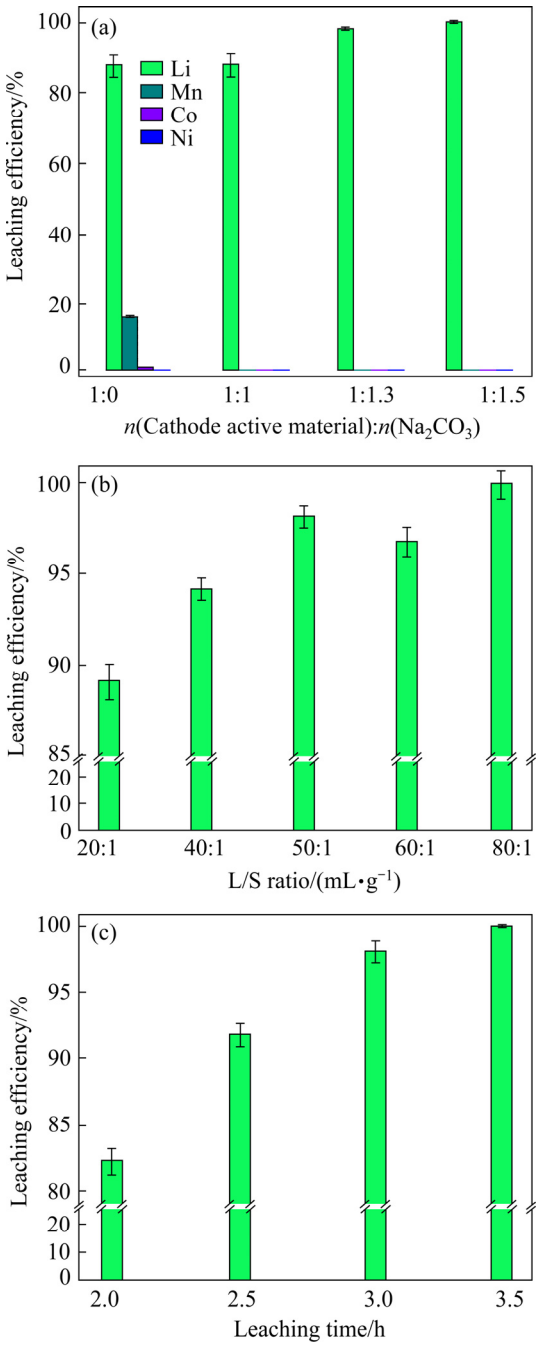

Fig. 6 Effect of molar ratio of cathode materials to Na_2CO_3 on leaching efficiencies of Li, Ni, Co, and Mn (a) and effects of liquid-to-solid ratio (b), and leaching time (c) on leaching efficiency of Li

to dissolve more Li_2CO_3 when the liquid-to-solid ratio was less than 50:1, resulting in a lower Li leaching efficiency. With an increase in the liquid-to-solid ratio, the leaching efficiency of Li also increased and then tended to level off. In this experiment, the optimal liquid-to-solid ratio was selected as 50:1.

The effect of the leaching time on the leaching efficiency of Li is shown in Fig. 6(c). The time is positively related to the leaching efficiency of Li. When the leaching time was 3 h, the leaching efficiency of Li reached 98.1%. The leaching efficiencies of Al^{3+} and Cu^{2+} were not discussed in the experimental results because the Cu^{2+} content was less than 0.012 mg/g, and no Al^{3+} was detected.

3.1.5 Characterization of Li_2CO_3 and Na_2CO_3 leaching residue

The XRD patterns of the recovered Li_2CO_3 and Na_2CO_3 leaching residue are shown in Figs. 7(a, b), respectively. From Fig. 7(a), it could be observed that the diffraction peaks of the recovered Li_2CO_3 were in good agreement with the diffraction peaks of the standard Li_2CO_3. At the same time, no other impurities were detected. Compared with the XRD pattern (Fig. 1(b)) of the post-roasted cathode materials, the diffraction peaks of Li_2SO_4 disappeared, and only the weak diffraction peak of Li_2CO_3 was observed from the XRD pattern of Na_2CO_3 leaching residue. The diffraction peaks of $CoCO_3$, $NiCO_3$, Co_3O_4, Mn_3O_4, MnO_2 and $(NiO)_m{\cdot}(MnO)_n$ were also detected in Na_2CO_3 leaching residue, which proved that Li was successfully and preferentially leached via Na_2CO_3 leaching process.

The SEM image and EDS results of the Na_2CO_3 leaching residue are shown in Figs. 8(a, b), respectively. The morphology of the leaching residue was almost spherical, which mainly corresponded to the destruction of the cathode material structure during the reductive roasting. Obvious lamellar morphology of the carbon element was observed in the SEM image, which was due to the formation of carbonate precipitation during the Na_2CO_3 leaching process. The same distribution of C and O was also clearly observed in the EDS spectra of the leaching residue, proving the formation of carbonate.

3.2 Ammonia leaching of Ni and Co

3.2.1 Effect of ammonia leaching parameters on leaching efficiency of Ni, Co, and Mn

The effects of ammonia leaching parameters on the leaching efficiencies of Ni, Co, and Mn are shown in Fig. 9. Under different experimental conditions, the contents of Cu^{2+} were all less than 0.06%, and no Al^{3+} was detected. The effect of leaching time on the leaching efficiencies of Ni, Co, and Mn was investigated with 3 mol/L of $(NH_4)_2CO_3$, 0.5 mol/L of Na_2SO_3, 4 mol/L of $NH_3{\cdot}H_2O$, at temperature of 80 °C and liquid-to-solid ratio of 40:1. As shown in Fig. 9(a), the leaching efficiency of Mn was less than 0.2% for different ammonia leaching time. With an increase in the leaching time, the leaching efficiencies of Ni and Co gradually increased and then stabilized. At 5 h, the leaching efficiencies of Ni and Co were higher, reaching 99.5% and 99.9%, respectively.

$NH_3{\cdot}H_2O$ and $(NH_4)_2CO_3$ were used as the complexes to provide an ammonia source in the ammonia leaching solution. The effect of the $(NH_4)_2CO_3$ dosage on the leaching efficiencies of Ni, Co, and Mn was investigated. As shown in Fig. 9(b), the leaching efficiency of Mn was below 0.12%. With an increase in the $(NH_4)_2CO_3$ dosage from 1 to 3 mol/L, the leaching efficiencies of Ni and Co increased from 81.4% and 85.2% to 99.5% and 99.9%, respectively. This could be attributed to the additional sources of ammonia which could react with Ni and Co. When the $(NH_4)_2CO_3$ dosage was continuously increased, the leaching efficiencies of Ni and Co became steady.

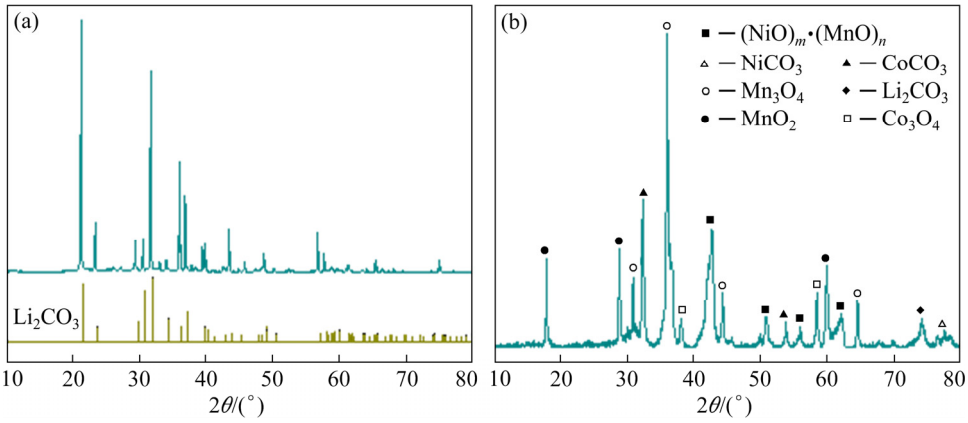

Fig. 7 XRD patterns of recovered Li_2CO_3 (a) and Na_2CO_3 (b) leaching residue

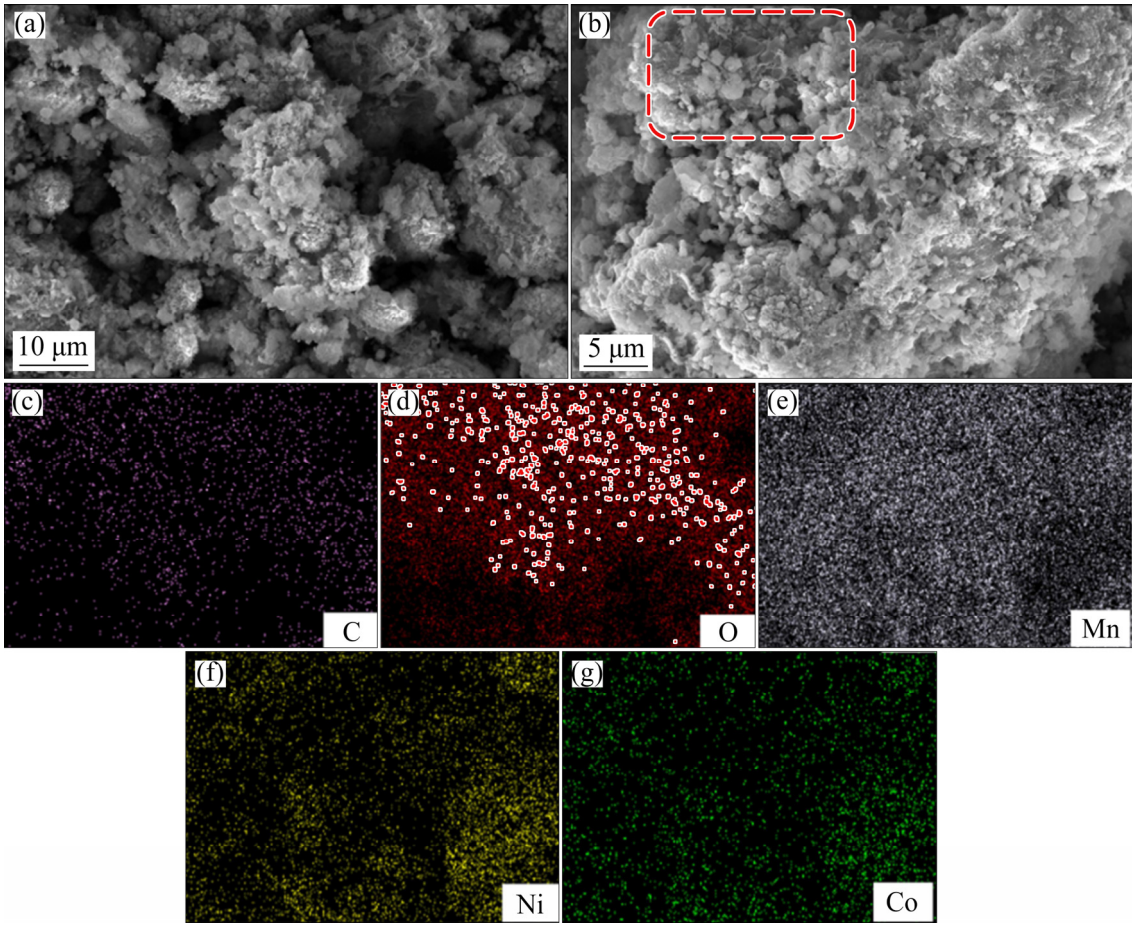

Fig. 8 SEM image (a) and EDS results (b−g) of Na_2CO_3 leaching residue

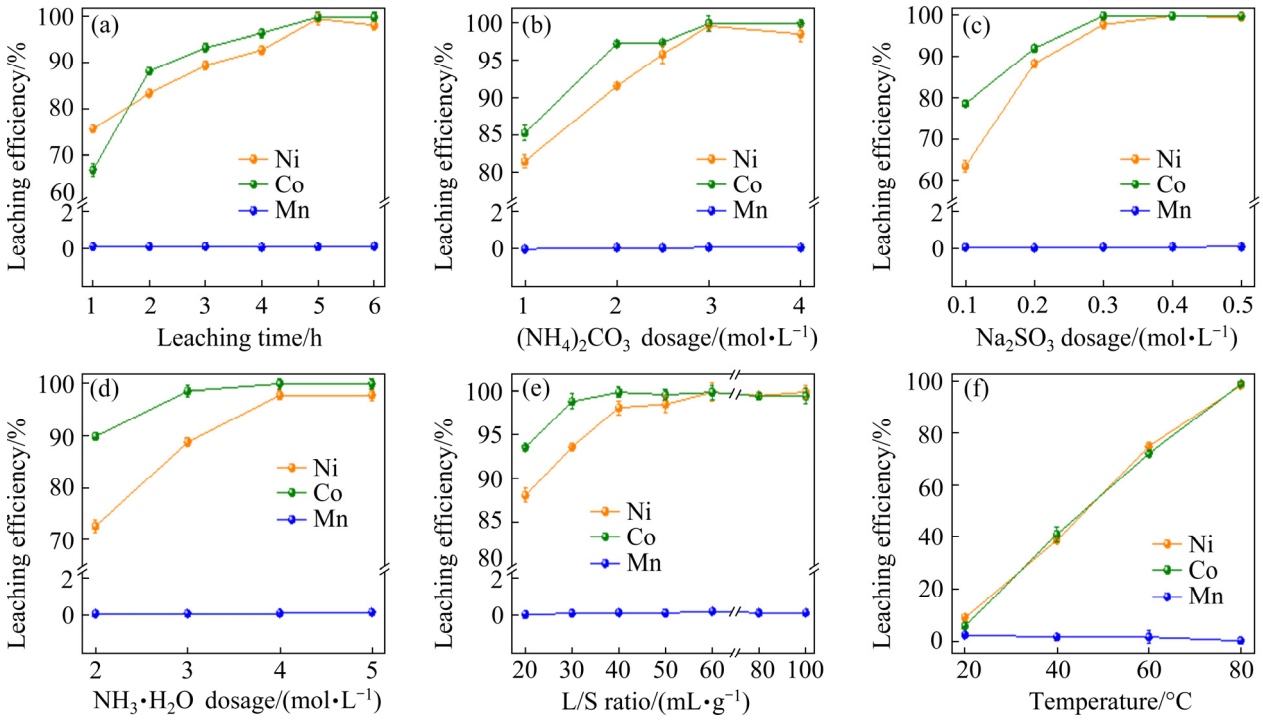

Fig. 9 Effects of leaching time (a), $(NH_4)_2CO_3$ dosage (b), Na_2SO_3 dosage (c), $NH_3·H_2O$ dosage (d), liquid-to-solid ratio (e) and temperature (f) on leaching efficiencies of Ni, Co, and Mn

XRD and XPS showed that the Co and Mn were still in a high valence state after reductive roasting, so they could not react with ammonia during ammonia leaching. Therefore, a small amount of reductant needed to be added to the ammonia leaching solution. The effect of the Na_2SO_3 dosage on the leaching efficiencies of Ni, Co, and Mn is shown in Fig. 9(c). It was found that the leaching efficiencies of Ni and Co were significantly improved by adding a reducing agent. When the Na_2SO_3 dosage was 0.1 mol/L, the leaching efficiencies of Ni and Co were only 63.4% and 78.6%, respectively. By increasing the dosage of the reducing agent, high-valence Co and Mn were fully reduced and reacted with ammonia to form soluble complexes. However, the complexes of Mn were unstable and changed into $MnCO_3$ precipitates along with CO_3^{2-} in the ammonia leaching solution, so the leaching efficiency of Mn was less than 0.15%. The leaching efficiencies of Ni and Co remained relatively stable when the Na_2SO_3 dosage was more than 0.3 mol/L. In the subsequent experiments, the Na_2SO_3 dosage was selected as 0.3 mol/L.

The effect of the $NH_3{\cdot}H_2O$ dosage on the leaching efficiencies of Ni, Co, and Mn is shown in Fig. 9(d). The leaching efficiency of Mn is always low (approximately 0.1%). The leaching efficiency of Co was significantly higher than that of Ni at $NH_3{\cdot}H_2O$ dosage less than 4 mol/L. The leaching efficiencies of Ni and Co tended to be the same when the dosage of $NH_3{\cdot}H_2O$ was higher than 4 mol/L. With an increase in the $NH_3{\cdot}H_2O$ dosage, more ammonia was added to complex Ni and Co, thereby increasing the leaching efficiencies of Ni and Co. When the dosage of $NH_3{\cdot}H_2O$ was 4 mol/L, the leaching efficiencies of Ni and Co were 97.8% and 99.9%, respectively, and tended to be stable.

The effect of the liquid-to-solid ratio on the leaching efficiencies of Ni, Co, and Mn is shown in Fig. 9(e). The leaching efficiency of Mn was less than 0.25%. With an increase in the liquid-to-solid ratio, the contact area among ions increased, and the leaching efficiencies of Ni and Co first increased and then became steady. At 30:1, the leaching efficiency of Co reached 98.8%, but the leaching efficiency of Ni was only 93.6%. At 40:1, the leaching efficiencies of Ni and Co were higher, reaching 98.1% and 99.9%, respectively.

The effect of temperature on the leaching efficiencies of Ni, Co, and Mn is shown in Fig. 9(f). The leaching efficiencies of Mn at 20, 40, and 60 °C were 2.4%, 1.6%, and 1.6%, respectively. However, the leaching efficiency of Mn was only 0.15% at 80 °C. This was attributed to the slower reaction rate at lower temperatures and the slower precipitation formation, which caused more Mn^{2+} to remain in the ammonia leaching solution. In addition, temperature had a significant influence on the leaching efficiencies of Ni and Co, and the leaching efficiency was positively and linearly correlated with temperature, which was attributed to the accelerated reaction rate and the increased frequency of molecular collisions.

3.2.2 Composition of ammonia leaching residue

Ni and Co could be selectively leached by ammonia, and Mn was recovered as $MnCO_3$ from the ammonia leaching residue. The XRD pattern of the ammonia leaching residue is shown in Fig. 10. It could be seen that the diffraction peaks of the ammonia leaching residue were in line with the characteristic diffraction peaks of $MnCO_3$; only small amounts of Mn_3O_4 and Al_2O_3 were detected in the ammonia leaching residue, and the characteristic peaks of existing impurities were not detected. Mn was recovered as $MnCO_3$ in this study.

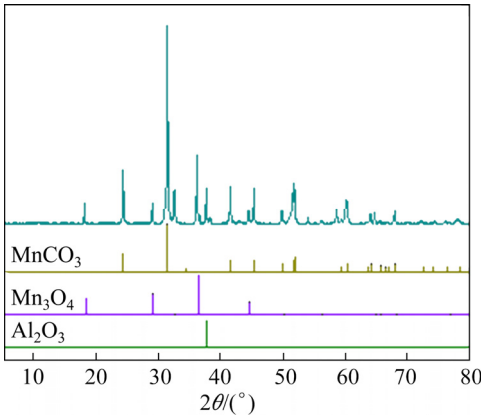

Fig. 10 XRD pattern of ammonia leaching residue

3.2.3 Kinetic analysis of ammonia leaching

To fully understand the kinetics of Ni and Co in the ammonia leaching process and to determine the control steps, the kinetics of the leaching of the cathode materials was explored at different temperatures. The kinetics of ammonia leaching was based on the shrinking core model. This experiment conformed to the three conditions of the shrinking core model: (1) The cathode materials were passed through a 325-mesh sieve after

grinding and had uniform particle size; (2) the liquid-to-solid ratio of the ammonia leaching experiments was 40:1, and the concentration of reactant was high; (3) From the SEM image of the Na_2CO_3 leaching residue of cathode materials (Fig. 8(a)), it was found that the materials used in the ammonia leaching experiments were dense and almost spherical. Therefore, the shrinking core model was suitable for this experiment. Chemical reaction control and internal diffusion control are the two most typical models in the shrinking core model, and the corresponding equations are shown in Eqs. (3) and (4), respectively. The activation energies of Ni and Co were calculated using the Arrhenius equation, as shown in Eq. (5):

$$1-(1-x)^{1/3}=k_1t \tag{3}$$

$$1-(2/3)x-(1-x)^{2/3}=k_2t \tag{4}$$

$$k=A\exp\left(\frac{-E_a}{RT}\right) \tag{5}$$

where k (min^{-1}) is the rate constant, t (min) is the leaching time, A (min^{-1}) is the frequency factor, E_a (J/mol) is the activation energy, R (8.314 J/(K·mol)) is the molar gas constant, and T (K) is the reaction temperature.

The leaching kinetic curves of Ni and Co were divided into two stages. The period of 0−60 min was considered as the first stage; the period of 60−300 min was considered the second stage of the ammonia leaching process. The data for Ni and Co in the ammonia leaching process were calculated using Eqs. (3) and (4): The chemical reaction control model was more suitable for the leaching process in this experiment than the internal diffusion control model. The fitting results of Ni and Co in 0−60 min and 60−300 min are listed in Table 2. The fitting results of the chemical reaction control model for Ni and Co at 20−80 °C are shown in Figs. 11(a, b), respectively. The activation energies of Ni and Co in 0−60 min were 29.1 and 29.3 kJ/mol, respectively (Fig. 11(c)), and in 60−300 min, they were 37.8 and 40.2 kJ/mol, respectively (Fig. 11(d)). The activation energies of 0−60 min were smaller than those in 60−300 min, because the cathode materials were reduced during the roasting process.

3.2.4 Mechanism of ammonia leaching

Ni, Co, and Mn can be effectively separated by ammonia leaching experiments. The ammonia leaching process is illustrated in Fig. 12. The ammonia leaching solution was maintained at a relatively stable pH through the ionization balance of $NH_3·H_2O$ and $(NH_4)_2CO_3$ in the ammonia leaching solution. A stable pH environment created a favorable complex environment for Ni, Co, and Mn to form stable complexes. The unreduced Ni, Co, and Mn in the roasting process were reduced to divalence by the reduction of Na_2SO_3. In the ammonia leaching solution, Ni^{2+}, Co^{2+}, and Mn^{2+} were complexed by free ammonia to form complexes of $Ni(NH_3)_n^{2+}$, $Co(NH_3)_n^{2+}$, and $Mn(NH_3)_n^{2+}$, respectively. $Ni(NH_3)_n^{2+}$ and $Co(NH_3)_n^{2+}$ existed stably in the ammonia leaching solution, while $Mn(NH_3)_n^{2+}$ was unstable and precipitated easily to form $MnCO_3$ with CO_3^{2-}, which is consistent with previous reports [27]. Relevant reports [11] indicated that, when the pH of the ammonia leaching solution was 8−10, $Ni(NH_3)_n^{2+}$ mainly existed as $Ni(NH_3)_4^{2+}$ and $Ni(NH_3)_5^{2+}$, and $Co(NH_3)_n^{2+}$ mainly existed as $Co(NH_3)_3^{2+}$, $Co(NH_3)_4^{2+}$, $Co(NH_3)_5^{2+}$, and $Co(NH_3)_6^{2+}$. The ammonia leaching reactions are shown as follows:

$$Ni^{2+}+nNH_3=Ni(NH_3)_n^{2+}\ (n=4,\ 5) \tag{6}$$

$$Co^{2+}+nNH_3=Co(NH_3)_n^{2+}\ (n=3,\ 4,\ 5,\ 6) \tag{7}$$

$$Mn^{2+}+nNH_3=Mn(NH_3)_n^{2+} \tag{8}$$

$$Mn(NH_3)_n^{2+}+CO_3^{2-}=MnCO_3\downarrow+nNH_3 \tag{9}$$

Table 2 Fitting results of chemical reaction control model for Ni and Co in 0−60 min and 60−300 min

T/K	Ni				Co			
	0−60 min		60−300 min		0−60 min		60−300 min	
	k_1/min^{-1}	R^2	k_1/min^{-1}	R^2	k_1/min^{-1}	R^2	k_1/min^{-1}	R^2
293.15	0.000433	0.99567	0.000108	0.98315	0.000485	0.95362	0.000099	0.99635
313.15	0.000958	0.99088	0.000359	0.99338	0.001040	0.95206	0.000334	0.94772
333.15	0.001820	0.99678	0.000631	0.99725	0.002100	0.99091	0.000561	0.97992
353.15	0.003220	0.99010	0.001650	0.99518	0.003730	0.99601	0.001890	0.99076

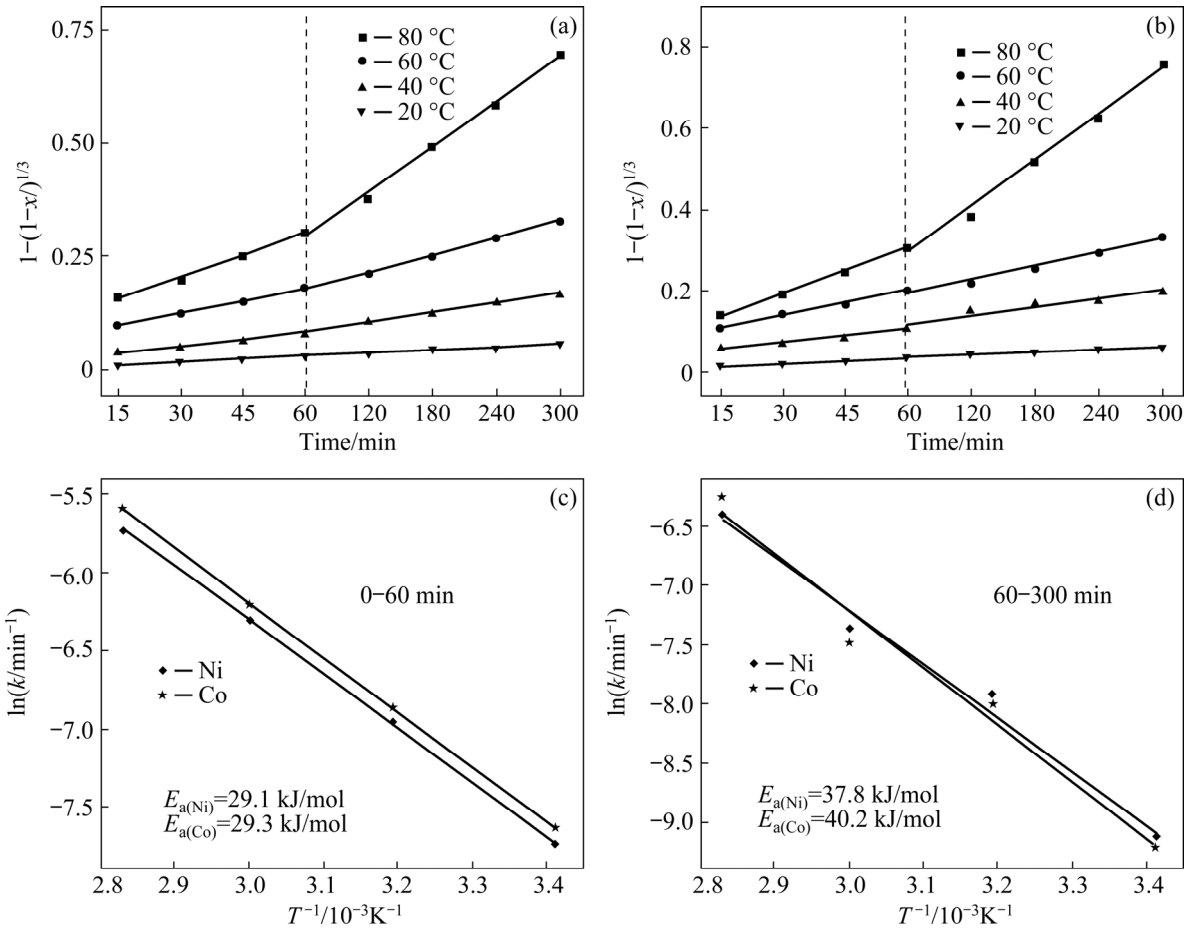

Fig. 11 Relationship between $1-(1-x)^{1/3}$ and time for Ni (a) and Co (b) at 20−80 °C in leaching; Arrhenius plots of Ni and Co in 0−60 min (c) and 60−300 min (d) at 20−80 °C for leaching

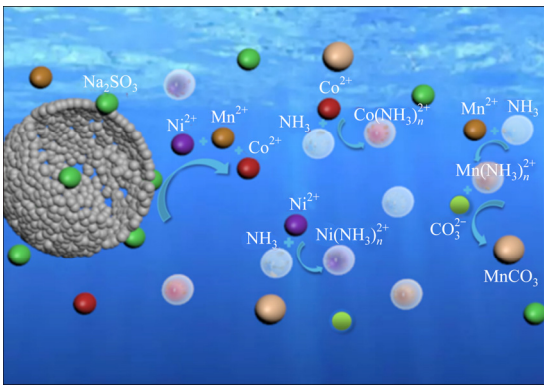

Fig. 12 Ammonia leaching process

3.3 Comprehensive experiments

To improve the leaching efficiencies of metals in LIB cathode materials, the reductive roasting conditions, Na_2CO_3 leaching conditions, and ammonia leaching conditions were explored, and the optimal conditions were obtained. Three sets of parallel experiments were performed under optimal conditions. The leaching efficiencies of the valuable metals are given in Table 3. In the Na_2CO_3 leaching experiments, the leaching efficiency of Li was above 99%, and the leaching efficiencies of Ni, Co, and Mn were below 0.5%, proving that Li could be preferentially leached. The leaching efficiencies of Ni and Co in the ammonia leaching experiments also exceeded 99%, and trace amounts of Cu were detected in the Na_2CO_3 leaching solution and ammonia leaching solution, but no Al was detected. In addition, pH changes were detected with time in the ammonia leaching solution of the three sets of parallel experiments under optimal conditions, as shown in Fig. 13. It was found that the pH of the ammonia leaching solution remained in a relatively stable state, proving that the ionization balance of $NH_3{\cdot}H_2O$ and $(NH_4)_2CO_3$ was effective at maintaining a stable pH. Meanwhile, Ni and Co were selectively leached via reductive roasting, Na_2CO_3 leaching, and ammonia leaching experiments. Mn and Al were leached in very small quantities. The leaching efficiencies of Ni and Co in

Table 3 Leaching efficiencies of valuable metals under optimal conditions

Metal	Leaching efficiency in sodium carbonate leaching experiment/%			Leaching efficiency in ammonia leaching experiment/%		
	No. 1	No. 2	No. 3	No. 1	No. 2	No. 3
Li	99.08	99.03	99.12	0.90	0.92	0.86
Ni	0.010	0.011	0.010	99.38	99.01	99.76
Co	0.028	0.028	0.029	99.9	99.47	99.89
Mn	0.009	0.007	0.008	0.036	0.051	0.067

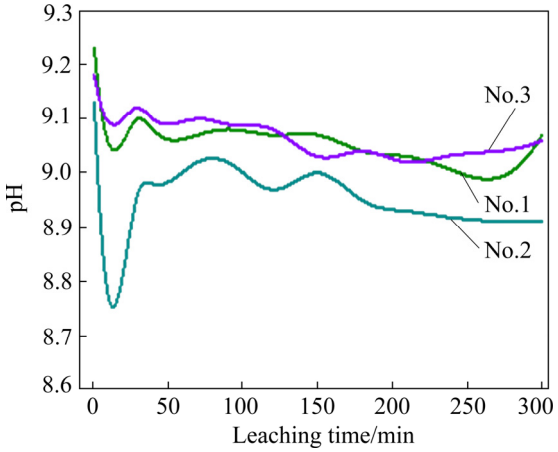

Fig. 13 pH changes with time under optimal conditions

this experiment were higher than those reported in other literature [11,13].

3.4 Recovery process of spent cathode materials

Aiming at the environmental risks and economic benefits of spent LIB cathode materials, an efficient and novel strategy for recovering valuable metals from cathode materials was proposed. The recovery process of the cathode materials from spent LIBs is shown in Fig. 14. The high-valence Ni, Co, and Mn in the cathode materials were reduced to a low-valence state via reductive roasting. Li was preferentially recovered as Li_2CO_3 by Na_2CO_3 leaching, and the leaching efficiency of Li reached more than 99%. Ni and Co were selectively leached through ammonia leaching experiments, and Mn was recovered as $MnCO_3$ precipitates. Ni and Co reacted with free ammonia in the ammonia leaching solution to form water-soluble complexes; the leaching efficiencies of Ni and Co were more than 99%. The ammonia leaching solution containing Ni and Co could be used to re-prepare the cathode materials. Ammonia did not need to be added to complex Ni, Co, and Mn when preparing the cathode materials.

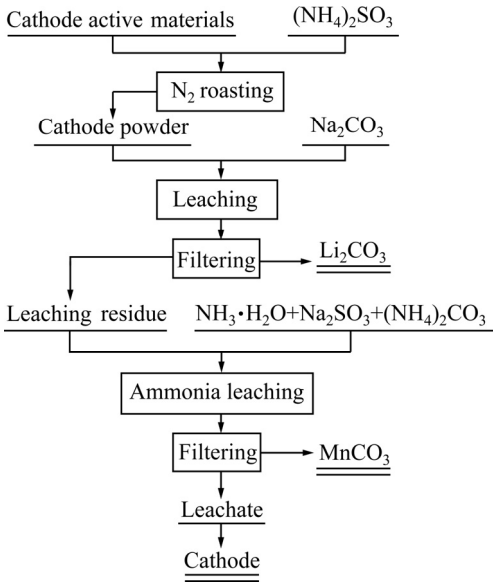

Fig. 14 Recovery process of cathode materials for spent LIBs

4 Conclusions

(1) The high-valence Ni, Co, and Mn in the cathode materials were reduced to a low-valence state via reductive roasting, and the mineral phase of the cathode material was reconstructed. Subsequently, Li was preferentially recovered in the form of Li_2CO_3 via Na_2CO_3 leaching. The leaching efficiency of Li exceeded 99%.

(2) Ni and Co were recovered via ammonia leaching. Ni (99.7%) and Co (99.9%) could be selectively leached through one-step ammonia leaching, while Mn could not be leached, proving that ammonia leaching had good selectivity. Mn was recovered as $MnCO_3$ precipitates.

(3) The kinetic study of Ni and Co showed that the leaching of Ni and Co conformed to the chemical reaction control. The activation energies of Ni and Co in 0−60 min were 29.1 and 29.3 kJ/mol, respectively, and in 60−300 min were 37.8 and 40.2 kJ/mol, respectively.

Acknowledgments

The authors are grateful for the financial support from the Focus on Research and Development Plan in Shandong Province, China (No. 2017GSF16102).

References

[1] MENG Fei, LIU Qing-cai, KIM R, WANG Jing-xiu, LIU Gui, GHAHREMAN A. Selective recovery of valuable metals from industrial waste lithium-ion batteries using citric acid under reductive conditions: Leaching optimization and kinetic analysis [J]. Hydrometallurgy, 2020, 191: 105160.

[2] LV Hong, HUANG Hai-jian, HUANG Cheng, GAO Qiang, YANG Ze-heng, ZHANG Wei-xin. Electric field driven de-lithiation: A strategy towards comprehensive and efficient recycling of electrode materials from spent lithium ion batteries [J]. Applied Catalysis B: Environmental, 2021, 283: 119634.

[3] REN Guo-xing, XIAO Song-wen, XIE Mei-qiu, PAN Bing, CHEN Jian, WANG Feng-gang, XIA Xing. Recovery of valuable metals from spent lithium ion batteries by smelting reduction process based on FeO−SiO_2−Al_2O_3 slag system [J]. Transactions of Nonferrous Metals Society of China, 2017, 27: 450−456.

[4] CAO Ning, ZHANG Ya-li, CHEN Lin-lin, CHU Wei, HUANG Yao-guo, JIA Yun, WANG Ming. An innovative approach to recover anode from spent lithium-ion battery [J]. Journal of Power Sources, 2020, 483: 229163.

[5] YANG Jian, JIANG Liang-xing, LIU Fang-yang, JIA Ming, LAI Yan-qing. Reductive acid leaching of valuable metals from spent lithium-ion batteries using hydrazine sulfate as reductant [J]. Transactions of Nonferrous Metals Society of China, 2020, 30: 2256−2264.

[6] ZHANG Ya-li, CHU Wei, CHEN Xia, WANG Ming, CUI Hong-you, WANG Jing. Recovery of rare earth metals and synthesis of $Ni_{0.6}Co_{0.2}Mn_{0.2}(OH)_2$ from spent asymmetric-capacitance power batteries [J]. Journal of Cleaner Production, 2019, 235: 1295−1303.

[7] JIA Li-pan, HUANG Jiang-jiang, MA Ze-long, LIU Xu-heng, CHEN Xing-yu, LI Jiang-tao, HE Li-hua, ZHAO Zhong-wei. Research and development trends of hydrometallurgy: An overview based on Hydrometallurgy literature from 1975 to 2019 [J]. Transactions of Nonferrous Metals Society of China, 2020, 30: 3147−3160.

[8] WANG Shu-bin, WANG Chao, LAI Feng-jiao, YAN Feng, ZHANG Zuo-tai. Reduction-ammoniacal leaching to recycle lithium, cobalt, and nickel from spent lithium-ion batteries with a hydrothermal method: Effect of reductants and ammonium salts [J]. Waste Management, 2020, 102: 122−130.

[9] LOU Wen-bo, ZHANG Yang, ZHANG Ying, ZHENG Shi-li, SUN Pei, WANG Xiao-jian, LI Jian-zhong, QIAO Shan, ZHANG Yi, WENZEL M, WEIGAND J. Leaching performance of Al-bearing spent $LiFePO_4$ cathode powder in H_2SO_4 aqueous solution [J]. Transactions of Nonferrous Metals Society of China, 2021, 31: 817−831.

[10] REFIY S, FLOWERI O, MAYANGSARI T, AIMEN A, ISKANDAR F. Green recycle processing of cathode active material from $LiNi_{1/3}Co_{1/3}Mn_{1/3}O_2$ (NCM 111) battery waste through citric acid leaching and oxalate co-precipitation process [J]. Materials Today: Proceedings, 2021, 44: 3378−3380.

[11] ZHENG Xiao-hong, GAO Wen-fang, ZHANG Xi-hua, HE Ming-ming, LIN Xiao, CAO Hong-bin, ZHANG Yi, SUN Zhi. Spent lithium-ion battery recycling–Reductive ammonia leaching of metals from cathode scrap by sodium sulphite [J]. Waste Management, 2017 60: 680−688.

[12] QI Ya-ping, MENG Fan-song, YI Xiao-xia, SHU Jian-cheng, CHEN Meng-jun, SUN Zhi, SUN Shu-hui, XIU Fu-rong. A novel and efficient ammonia leaching method for recycling waste lithium ion batteries [J]. Journal of Cleaner Production, 2020, 251: 119665.

[13] WU Cai-bin, LI Ben-sheng, YUAN Cheng-fang, NI Shuai-nan, LI Li-feng. Recycling valuable metals from spent lithium-ion batteries by ammonium sulfite-reduction ammonia leaching [J]. Waste Management, 2019, 93: 153−161.

[14] WANG Chao, WANG Shu-bin, YAN Feng, ZHANG Zhen, SHEN Xue-hua, ZHANG Zuo-tai. Recycling of spent lithium-ion batteries: Selective ammonia leaching of valuable metals and simultaneous synthesis of high-purity manganese carbonate [J]. Waste Management, 2020, 114: 253−262.

[15] MA Ya-yun, TANG Jing-jing, WANALDI R, ZHOU Xiang-yang, WANG Hui, ZHOU Chang-you, YANG Juan. A promising selective recovery process of valuable metals from spent lithium ion batteries via reduction roasting and ammonia leaching [J]. Journal of Hazardous Materials, 2021, 402: 123491.

[16] MENG Xiang-qi, HAO Jie, CAO Hong-bin, LIN Xiao, NING Peng-ge, ZHENG Xiao-hong, CHANG Jun-jun, ZHANG Xi-hua, WANG Bao, SUN Zhi. Recycling of $LiNi_{1/3}Co_{1/3}Mn_{1/3}O_2$ cathode materials from spent lithium-ion batteries using mechanochemical activation and solid-state sintering [J]. Waste Management, 2019, 84: 54−63.

[17] DENNY Y, LEE K, PARK C, OH S, KANG H, YANG D, SEO S. Electronic, electrical and optical properties of undoped and Na-doped NiO thin films [J]. Thin Solid Films, 2015, 591: 255−260.

[18] BAI Hong-ye, LI Xia, ZHAO Yong, FAN Wei-qiang, LIU Ying, GAO Yang, XU Dong-bo, DING Jin-rui, SHI Wei-dong. Fabrication of $BiVO_4$−Ni/Co_3O_4 photoanode for enhanced photoelectrochemical water splitting [J]. Applied Surface Science, 2021, 538: 148150.

[19] SHALABI K, El-GAMMAL O, ABDALLAH Y. Adsorption and inhibition effect of tetraaza−tetradentate macrocycle ligand and its Ni(II), Cu(II) complexes on the corrosion of $Cu_{10}Ni$ alloy in 3.5% NaCl solutions [J]. Colloids and Surfaces A: Physicochemical and Engineering Aspects, 2021, 609: 125653.

[20] YI Hong-hong, YANG Zhong-yu, TANG Xiao-long, ZHAO Shun-zheng, GAO Feng-yu, WANG Jian-gen, HUANG Yong-hai, MA Yue-qiang, CHU Chao, LI Qian, XU Jia-li. Promotion of low temperature oxidation of toluene vapor derived from the combination of microwave radiation and

nano-size Co_3O_4 [J]. Chemical Engineering Journal, 2018, 333: 554−563.

[21] WANG Zi-ying, SUN Jing-yao, HUO Yan-ming, YAN Yu-hua, MA Zong-tao, BU Miao-miao, SUN Chun, HUA Zhong-qiu, YANG Xue-li, BI Wen-gang, ZHANG Tong. Porous Co_3O_4 nanocrystals derived by metal-organic frameworks on reduced graphene oxide for efficient room-temperature NO_2 sensing properties [J]. Journal of Alloys and Compounds, 2021, 856: 158199.

[22] ABD-EIRAHIM A, CHUN D. Nanosized Co_3O_4–MoS_2 heterostructure electrodes for improving the oxygen evolution reaction in an alkaline medium [J]. Journal of Alloys and Compounds, 2021, 853: 156946.

[23] LIU Ruo-yu, ZHOU Bing, LIU Li-zhong, ZHANG Yan, CHEN Yu, ZHANG Qiao-ling, YANG Ming-liang, HU Lan-ping, WANG Miao, TANG Yan-feng. Enhanced catalytic oxidation of VOCs over porous Mn-based mullite synthesized by in-situ dismutation [J]. Journal of Colloid and Interface Science, 2021, 585: 302−311.

[24] YE Kai-hang, LIU Zhao-qing, XU Chang-wei, LI Nan, CHEN Yi-bo, Su Yu-Zhi. MnO_2/reduced graphene oxide composite as high-performance electrode for flexible supercapacitors [J]. Inorganic Chemistry Communications, 2013, 30: 1−4.

[25] WANG Z H, GENG D Y, ZHANG Y J, ZHANG Z D. Morphology, structure and magnetic properties of single-crystal Mn_3O_4 nanorods [J]. Journal of Crystal Growth, 2008, 310: 4148−4151.

[26] ZHANG Li, LIU Bing-bing, ZHANG Yuan-bo, HAN Gui-hong, HUANG Jun-jie, YE Jing, LI Yue-long. New perspective on the interface reaction and morphology evolution in the reduction of manganese silicate for silicomanganese alloy production [J]. Applied Surface Science, 2021, 539: 148210.

[27] WANG Hong-yan, HUANG Kai, ZHANG Yang, CHEN Xin, JIN Wei, ZHENG Shi-li, ZHANG Yi, LI Ping. Recovery of lithium, nickel, and cobalt from spent lithium-ion battery powders by selective ammonia leaching and an adsorption separation system [J]. ACS Sustainable Chemistry and Engineering, 2017, 5: 11489−11495.

从废旧锂离子电池中优先回收锂并高效回收镍和钴

曹 宁，张亚莉，陈琳琳，贾 云，黄耀国

山东理工大学 化学化工学院，淄博 255049

摘 要：采用还原焙烧−碳酸钠浸出−氨浸出的方法对废旧锂离子电池正极材料进行回收处理。研究焙烧参数、Na_2CO_3 浸出参数和氨浸出参数对金属浸出率的影响。结果表明，还原焙烧过程中，废旧锂离子电池的矿相结构被重新构建，通过 Na_2CO_3 浸出过程，超过 99% 的锂被优先回收。通过一步氨浸出法可将 99.7%的镍和 99.9% 的钴浸出，而锰不能被浸出，表现出优异的选择性。动力学研究表明镍和钴的浸出符合化学反应控制。

关键词：锂；优先回收；还原焙烧；氨浸出；废旧锂离子电池

(Edited by Bing YANG)